Journal of the Chinese Society of Mechanical Engineers, Vol.47, No.4, pp309~317 (2026)

Mechanical Enhancement of PMMA/SiO_2: Quantitative Dispersion Analysis and Prediction

Cheng-En Jiang*, Guan-Yu Chen*and Shih-Chen Shi*,**

Keywords： Poly(methyl methacrylate) (PMMA), silica nanocomposites, finite element analysis, particle dispersion, mechanical properties

ABSTRACT

Poly(methyl methacrylate) (PMMA) bone cements suffer from insufficient mechanical strength, often leading to aseptic loosening and implant failure. To address this, PMMA/SiO_2 nanocomposites were synthesized via the in-situ sol-gel method, incorporating a quantitative dispersion index ($D_{0.2}$) to rigorously evaluate particle distribution. Real-microstructure Finite Element Analysis (FEA) was employed to simulate stress evolution and test the hypothesis that well-dispersed silica acts as a physical barrier to impede crack propagation. The results indicate that while agglomerates act as stress concentrators, triggering defect-controlled failure, uniform dispersion enhances stress transfer and facilitates crack deflection. The simulation framework, validated by experimental data, accurately projects theoretical mechanical limits at 100% dispersion. These findings establish a robust predictive model for optimizing the microstructural design of high-performance biomedical composites.

INTRODUCTION

Poly(methyl methacrylate) (PMMA) occupies a pivotal position in the biomedical materials market, distinguished by its excellent biocompatibility, processability, and chemical stability (Szczęsny et al., 2022; Szoradi et al., 2024). Since its transition from dentistry to orthopedics between 1950 and 1980, PMMA has established itself as the gold standard for bone cement in artificial joint replacements. A significant milestone was achieved in the 1970s with the introduction of antibiotic-loaded bone cements, which successfully reduced the rate of deep infection in arthroplasty from approximately 5% to less than 1% (Bistolfi et al., 2019; Jaeblon, 2010; Van Vugt et al., 2019). Moving into the 21st century, research focus has shifted toward developing multifunctional antimicrobial composites, optimizing controlled drug release, mitigating antibiotic resistance, and enhancing osseointegration (Ramanathan et al., 2024). Despite these advancements in biological functionality, the global demand for high-performance fixation materials continues to rise as the population ages.

While PMMA has evolved to address infection risks, its intrinsic mechanical strength and fracture toughness remain relatively insufficient (Karpiński & Szabelski, 2025). Under long-term exposure to complex physiological cyclic loading, the material is prone to fatigue crack initiation and propagation, leading to cement fragmentation (Nguyen et al., 1997; Race & Mann, 2008). This structural degradation is frequently cited as a primary cause of aseptic loosening and subsequent implant failure, thereby severely limiting the prosthesis's long-term service life. To overcome these limitations, incorporating inorganic nanofillers, such as silica, into the polymer matrix to fabricate organic-inorganic nanocomposites has emerged as a robust strategy to enhance stiffness and durability (Kontou et al., 2023; Li et al., 2022).

However, the ultimate performance of these nanocomposites is critically dependent on the dispersion state of the inorganic fillers. Due to their high specific surface energy, nanoparticles are highly susceptible to agglomeration within the matrix (Sui et al., 2022). Micromechanical studies indicate that these agglomerates often act as stress concentrators, defects that accelerate material failure rather than preventing it. To address this, have increasingly utilized microstructure-based finite element analysis (FEA) to bridge the gap between stochastic particle distributions and macroscopic fracture behavior (Grove et al., 2025; Zhu et al., 2025). Unlike idealized models, these advanced computational frameworks integrate real-microstructure geometries to simulate localized stress evolution, offering

Paper Received January, 2026. Revised March, 2026. Accepted March, 2026. Author for Correspondence: Shih-Chen Shi.

* *Student, Department of Mechanical Engineering, National Cheng Kung University, 70101 Tainan, Taiwan*

** *Professor, Department of Mechanical Engineering, National Cheng Kung University, 70101 Tainan, Taiwan*

insights into how specific dispersion states influence crack initiation. Consequently, quantifying the degree of dispersion and elucidating its correlation with failure mechanisms remains a critical challenge in the design of high-performance biomedical composites (Abhiram & Ghosh, 2023; Karbowniczek et al., 2022; Shi et al., 2020).

Based on reinforcement mechanisms that demonstrate how particle addition alters mechanical properties, this study explores PMMA/SiO_2 composites, hypothesizing that dispersed silica acts as a physical barrier to impede crack growth (Bokobza, 2023; Chrispin Laila et al., 2022; Shi & Zeng, 2022; Zhong et al., 2025). Real-microstructure FEA was employed for prediction, while in-situ sol-gel synthesis and a quantitative dispersion index ($D_{0.2}$) were utilized to experimentally verify the correlation between particle distribution and mechanical performance.

MATERIALS PREPARATION AND EXPERIMENTAL PROCEDURE

Materials Preparation

The sol-gel method to prepare PMMA/SiO_2 composites effectively controls the generation and dispersion of the inorganic phase. In the preparation of the inorganic phase, tetraethoxysilane (TEOS) served as the precursor, with ethanol as the solvent and ammonia as the catalyst; SiO_2 nanoparticles were generated through hydrolysis and condensation, with their size and yield controlled by adjusting the TEOS concentration (5, 7, and 10 wt%), reaction temperature, and time. The specific experimental parameters and corresponding sample designations are summarized in Table 1. Concurrently, for the organic phase, PMMA powder was dissolved in tetrahydrofuran (THF), into which benzoyl peroxide (BPO) and the silane coupling agent 3-(trimethoxysilyl)propyl methacrylate (MPTS) were added; MPTS functioned as a bridge to enhance compatibility by bonding its hydrophobic end to the PMMA and its hydrophilic end to the hydroxyl groups on the SiO_2 surface. Finally, the inorganic solution was slowly mixed into the organic phase. After solvent removal by reduced-pressure concentration, the mixture was cast into Teflon molds and cured at 60°C for 24 hours (Jiang et al., 2025).

Table 1. Experimental parameters and corresponding sample designations for PMMA/SiO_2 composites.

Sample	Code Name
5 wt%+0.01 M+20°C +90 min	P5N012090
5 wt%+0.05 M+40°C +180 min	P5N0540180
5 wt%+0.1 M+60°C +270 min	P5N160270
7 wt%+0.01 M+40°C +270 min	P7N0140270
7 wt%+0.05 M+60°C +90 min	P7N056090
7 wt%+0.1 M+20°C +180 min	P7N120180
10 wt%+0.01 M+60°C +180 min	P10N0160180
10 wt%+0.05 M+20°C +270 min	P10N0520270
10 wt%+0.1 M+40°C +90 min	P10N14090
5 wt%+0.1 M+60°C +180 min	P5N160180

Mechanical Testing

The prepared composite films were cut into dumbbell-shaped specimens with a gauge length of 6.75 mm. Uniaxial tensile tests were conducted using a micro-tensile testing machine (Kammrath & Weiss GmbH) at a strain rate of 2 μm/s. To ensure data reproducibility and statistical reliability, at least ten independent specimens were tested for each experimental condition. Load-displacement curves were recorded to calculate Young's modulus, tensile strength, and fracture strain.

Quantification of Particle Dispersion

To quantitatively evaluate the dispersion quality of silica nanoparticles within the PMMA matrix, a statistical analysis based on Voronoi tessellation was employed. Cross-sectional SEM images were first processed in ImageJ; the images were binarized to clearly distinguish the silica particles from the polymer matrix. Subsequently, Voronoi diagrams were constructed, where each polygon defines the local area available to a particle. Dispersion homogeneity was characterized by the dispersion index $D_{0.2}$. This index is defined as the percentage of the Voronoi polygon areas that fall within ±20% of the mean polygon area (μ). Mathematically, D_k represents the probability of a polygon area (a) falling within the interval [μ(1-k), μ(1+k)]. The formulation is defined as shown in Equation (1):

$$D_k = \int_{\mu(1-k)}^{\mu(1+k)} f(a)da \quad (1)$$

A higher $D_{0.2}$ value indicates a more uniform spatial distribution of particles (equidistant dispersion), whereas a lower value suggests significant particle agglomeration or irregular distribution. The quantitative results of this analysis, including the calculated dispersion indices and average particle sizes for each experimental group, are summarized in Table 2.

Table 2. Analysis of particle size distribution and dispersion characteristics of PMMA/SiO_2 composites.

Code Name	$D_{0.2}$ (%)	Average particle size (nm)
P5N012090	22.52	118
P5N0540180	36.42	156
P5N160270	51.63	204
P7N0140270	20.53	260
P7N056090	24.5	200
P7N120180	32.32	238
P10N0160180	31.09	339
P10N0520270	32.45	435
P10N14090	40.33	332
P5N160180	55.73	148

Microstructural Mesh Generation

Object-oriented finite element software (OOF2) was utilized to convert cross-sectional SEM images of PMMA/SiO_2 composites, captured at 100k magnification (500 nm scale bar), into finite element mesh models. The process began with binarizing the images to differentiate the silica particles (black) from the PMMA matrix (white). Upon importing the images into OOF2, the physical dimensions were defined using ImageJ calibration data, and material pixels were assigned, confirming that the particle area percentage determined by OOF2 was consistent with the ImageJ analysis. Subsequently, an adaptive mesh skeleton was generated with a target element homogeneity index of 0.999. The skeleton was refined by moving nodes to meet this criterion, after which it was associated with material properties. The final mesh was then generated and exported to Abaqus software for further definition and analysis. The resulting finite element mesh reconstructions for the experimental samples are presented in Fig. 1.

Furthermore, given the limited dispersion range observed in the experimental samples, idealized binary images exhibiting equidistant, uniform, and varying degrees of aggregation were created. These idealized models were processed using the same workflow to facilitate a systematic investigation into the relationships among particle dispersion, particle size, and mechanical properties.

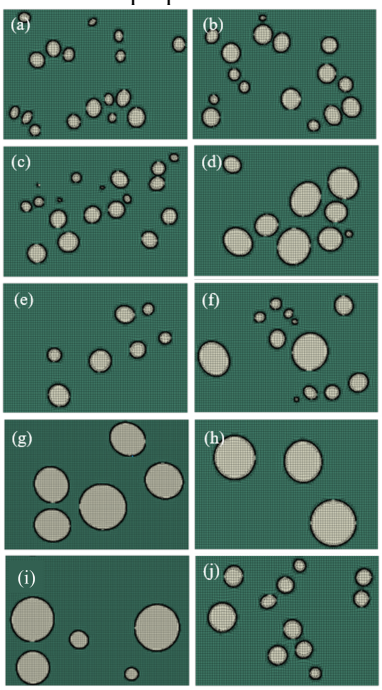

Fig. 1 Finite element mesh reconstructions of PMMA/SiO_2 microstructures at a 500 nm scale. Values in parentheses indicate the particle dispersion index ($D_{0.2}$ in):(a) 22.52, (b) 36.42, (c) 51.63, (d) 20.53, (e) 24.5, (f) 32.32, (g) 31.09, (h) 32.45, (i) 40.33, and (j) 55.73.

Finite Element Simulation Setup

The FEA was performed using the commercial software Abaqus/Explicit to study the micromechanical behavior of PMMA/SiO_2 composites under tensile loading. The simulation model was built from real microstructural images processed with OOF2 software. To ensure the model accurately represented the experimental material behavior, the engineering stress-strain data from macroscopic tensile tests were converted into true stress-strain curves. While the elastic modulus remained the same between the two curves, the plastic region needed recalibration; specifically, the true strain decreased while the true stress increased compared to the engineering data. These adjusted values for fracture strain and tensile strength were used as input parameters for the elastoplastic PMMA matrix. Simultaneously, the silica particles were modeled as a linear elastic material with a density of 1.95 g/cm³, a Young's modulus of 80 GPa, and a Poisson's ratio of 0.17. The models assumed a perfect interfacial bond between the silica nanoparticles and the PMMA matrix. This assumption is supported by our EDS and Raman spectroscopic results, which confirmed robust chemical coupling achieved through the in-situ sol-gel process. Although this simplifies the interfacial debonding phenomena, it allows for systematic examination of the effects of dispersion geometry ($D_{0.2}$) on the mechanical response.

Boundary conditions were applied using kinematic coupling constraints to simulate uniaxial tension, as illustrated in Fig. 2. Two reference points were established: one coupled to the nodes at the bottom edge and the other to the nodes at the top edge of the microstructure. The bottom reference point was fully constrained ($U_1=U_2=U_3=0$), while a displacement load (ΔL_{model}) derived from the experimental fracture strain was applied to the top reference point in the loading direction (U_2). Given the extremely fine mesh and material heterogeneity, which can lead to convergence issues in implicit solvers, an explicit dynamic analysis was adopted for a quasi-static simulation. To ensure that inertial effects were negligible and that the solution approximated a static state, a modal analysis was first performed to identify the microstructure's fundamental natural frequency. The time period for the explicit step was then determined from the inverse of this frequency, ensuring that the kinetic energy remained negligible relative to the internal energy throughout the deformation process.

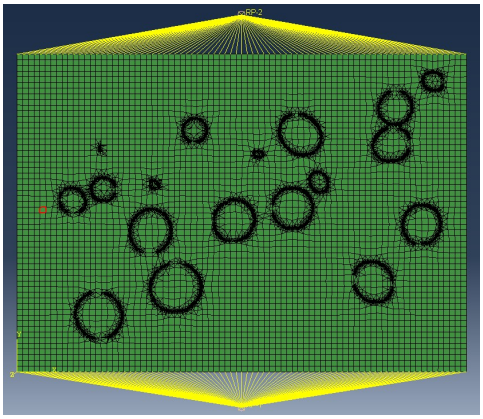

Fig. 2 Finite element mesh model illustrating the boundary conditions and kinematic coupling setup.

RESULTS AND DISCUSSION

Characterization of Material Structure

To confirm the chemical composition and structural integrity of the synthesized materials, Energy-dispersive X-ray Spectroscopy (EDS) and Raman spectroscopy were used. The elemental analysis of the synthesized particles via EDS revealed an atomic ratio of Oxygen to Silicon of approximately 67.7:32.3 and 70.1:29.9. While slightly deviating from the theoretical stoichiometric ratio of 2:1, these values fall within an acceptable error margin, confirming the synthesis of amorphous silica nanoparticles (Jiang et al., 2025).

Further structural characterization of the PMMA/SiO_2 composites was conducted using Raman spectroscopy to verify the grafting mechanism. The spectra showed enhanced vibrational peaks associated with PMMA (e.g., at 377, 603, 813, 1048, 1450, 1640, and 1764 cm^{-1}), indicating an increase in the degree of polymerization and the polymer chain size. Concurrently, variations in silica-related bands were observed; specifically, the intensity of bands at 460 and 711 cm^{-1}, associated with silica rings and Si-CO bonds, decreased, while the band at approximately 980 cm^{-1}, corresponding to Si-OH bonds, increased. These spectral shifts substantiate the successful grafting of SiO_2 particles onto the PMMA matrix and the formation of a robust organic-inorganic interface.

Material Model Calibration

To accurately simulate the mechanical behavior of composite materials in finite element analysis, the input material properties must be defined in terms of true stress and true strain to account for instantaneous geometric changes during large deformations. In this study, the engineering stress-strain curves obtained from the tensile tests were converted into true stress-strain curves, as illustrated in Fig. 3. The black curve represents the engineering stress-strain data, while the red curve represents the converted true stress-strain data. The curves in the elastic region overlap perfectly, indicating that Young's modulus remains unchanged after the conversion and does not need to be recalculated. However, upon entering the plastic region, significant deviations occur: compared to the engineering data, the true strain decreases while the true stress increases.

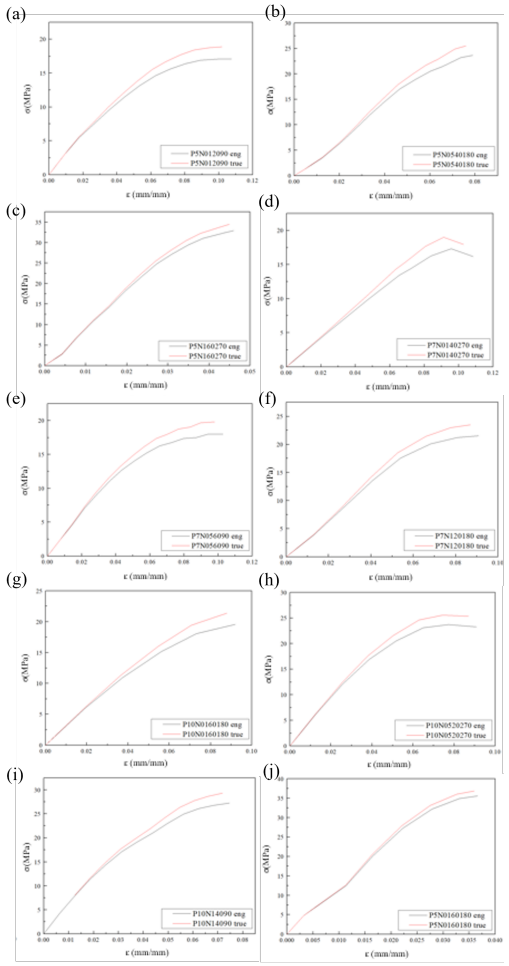

Fig. 3 Comparison of engineering and true stress-strain curves for PMMA/SiO_2 composites: (a) P5N012090, (b) P5N0540180, (c) P5N160270, (d) P7N0140270, (e) P7N056090, (f) P7N120180, (g) P10N0160180, (h) P10N0520270, (i) P10N14090, and (j) P5N160180V.

Microstructural Analysis

While macroscopic tensile testing confirms that the incorporation of silica particles effectively reinforces the PMMA matrix, it fails to provide direct observations of internal stress evolution and failure mechanisms. Consequently, this study employed FEA to simulate micromechanical behavior under varying dispersion and particle size conditions. The simulation results reveal two distinct failure regimes based on particle dispersion quality: defect-controlled and strength-limited fracture. The spatial distribution of particles and local agglomeration phenomena exert

a decisive influence on stress-transfer efficiency and failure modes (Fig. 5(a)-(c)).

The influence of particle distribution becomes evident when examining the impact of agglomeration and proximity. In samples characterized by poor dispersion or local agglomeration, failure consistently initiated at relatively low stress levels (17.55–23.40 MPa). This premature failure was driven by a defect-controlled mechanism, in which local agglomerates acted as critical stress-concentration sites rather than the material failing at its theoretical strength limit. For instance, in P5N012090 (Fig. 4(a)) and P7N120180 (Fig. 4(f)), severe stress gradients were observed near small agglomerates. While these clusters provided local reinforcement, the insufficient matrix material between closely spaced particles led to structural inhomogeneities, resulting in fracture perpendicular to the tensile direction. Similarly, even in samples with higher particle counts, such as P5N0540180 (Fig. 4(b)) and P5N160270 (Fig. 4(c)), the critical failure point was governed by the specific interaction between particle pairs or small clusters, with localized stress peaks reaching approximately 23.40 MPa before failure. This phenomenon is most evident in P7N0140270 (Fig. 4(d)) and P10N0160180 (Fig. 4(g)). Despite fair global dispersion, the extremely proximity of two critical particles created a preferential site for crack nucleation, causing cracks to propagate along the particle boundaries immediately upon initiation.

In contrast to the failure observed in agglomerated systems, samples exhibiting uniform particle dispersion demonstrated significantly superior load-bearing capabilities. In P7N056090 (Fig. 4 (e)), P10N0520270 (Fig. 4 (h)), and P10N14090 (Fig. 4 (i)), the stress was effectively distributed across the matrix, delaying fracture initiation. In these well-dispersed systems, the failure shifts to a strength-limited mode, where fracture typically initiates at the particle poles aligned with the tensile axis (the theoretical maximum stress point for spherical inclusions). This indicates that the composite failed due to the material reaching its intrinsic strength limit rather than defect-induced stress concentrations.

Cluster-Induced Reinforcement (Fig. 4 (j)). A unique phenomenon was observed in the optimal group, P5N160180 (Fig. 4 (j)), which achieved a high stress value of 26.19 MPa. Analysis reveals that the highest reinforcement efficiency did not stem from isolated particles, but from a localized cluster of three particles. Unlike the detrimental two-particle interactions observed in other groups, this triangular arrangement effectively dissipates stress and extends the crack propagation path, thereby enhancing energy dissipation. The proximity and geometric configuration of these three particles allow their individual stress fields to overlap, creating a localized reinforcement zone that redistributes the external load more effectively across the polymer matrix. This configuration mitigates the high-intensity stress concentration typically observed in the narrow ligaments between particle pairs. However, the crack still initiated at the periphery of this cluster, confirming that even in optimized systems, the stochastic formation of local particle neighbors remains the primary determinant of the ultimate failure location.

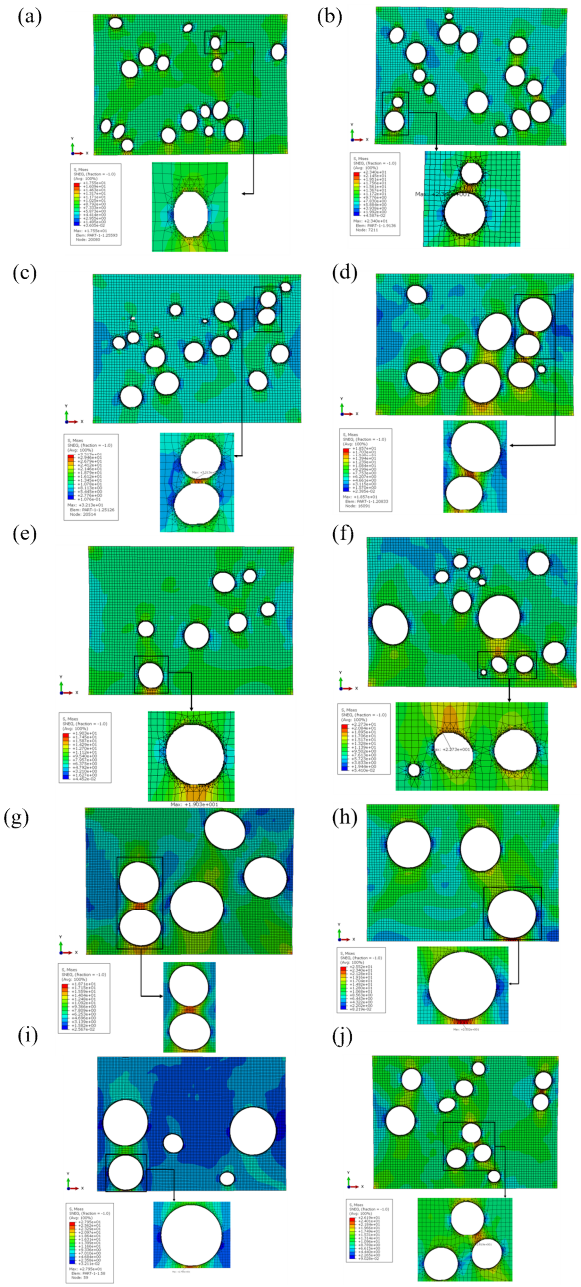

Fig. 4 Von Mises stress contours of PMMA/SiO_2 composites: (a) P5N012090, (b) P5N0540180, (c) P5N160270, (d) P7N0140270, (e) P7N056090, (f) P7N120180, (g) P10N0160180, (h) P10N0520270, (i) P10N14090, and (j) P5N160180V.

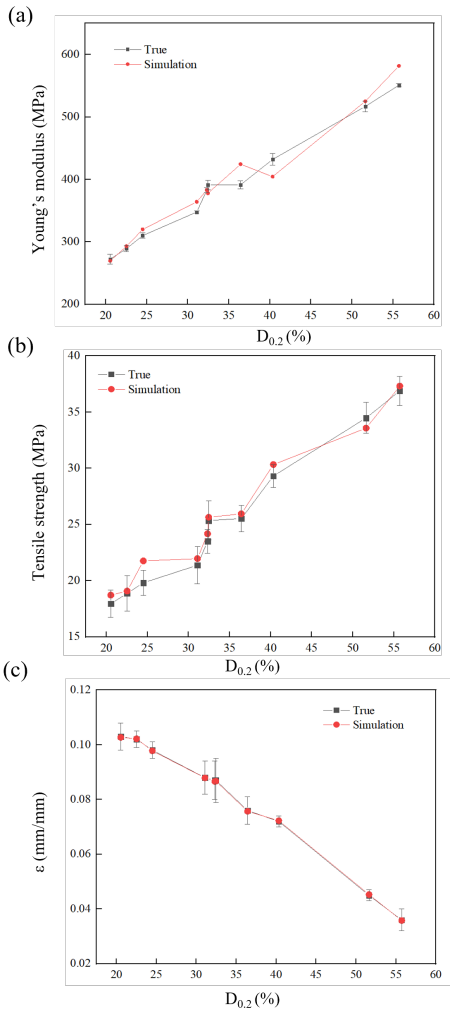

Fig. 5 Comparison of experimental and simulated results versus particle dispersion: (a) Young's modulus, (b) Tensile strength, and (c) Fracture strain, confirming model accuracy.

Prediction of Ideal Material Properties

Building upon the experimental results presented in the preceding sections, a pronounced correlation was observed between $D_{0.2}$ and the key mechanical properties. To elucidate the theoretical limits of material performance, this study established a predictive framework using a series of "idealized" microstructural states.

As illustrated in Fig. 6, twelve distinct finite element models were constructed to represent a full spectrum of dispersion scenarios. These models range from states of severe agglomeration (S) and large spherical clusters (LS) to intermediate phases (I) and, finally, to a theoretically perfect uniform distribution (U). Specifically, Fig. 6 (a)–(d) depicts the various dispersion arrangements for a 3 wt% loading of 100 nm particles; Fig. 6 (e)–(h) presents the configurations for the 5 wt% loading; and Fig. 6 (i)–(l) displays the results for the 7 wt% loading. This systematic variation across different weight percentages allows for the isolation of the dispersion effect from other experimental variables, facilitating a rigorous analysis.

The stress evolution within these idealized structures reveals distinct failure mechanisms. Figure 6 presents the Von Mises stress contours for three representative cases: a small triangular cluster (Fig. 7(a)), a large spherical agglomerate (Fig. 7(b)), and a uniform distribution (Fig. 7(c)). Consistent with experimental observations, the agglomerated models exhibit severe stress concentrations at the particle interstices, serving as potential crack initiation sites. In contrast, the uniform model demonstrates a homogeneous stress distribution, maximizing the load-bearing efficiency of the silica filler.

Finally, the quantitative data obtained from these simulations were synthesized to predict the ultimate mechanical potential of the composites. Fig. 8 illustrates the linear regression analysis correlating $D_{0.2}$ with Young's modulus, tensile stress, and fracture strain. The trends indicate a strong positive correlation between dispersion quality and mechanical strength/stiffness. By extrapolating these linear models to a $D_{0.2}$ of 100%, the theoretical upper limits of the mechanical properties for PMMA/SiO_2 composites under ideal dispersion conditions can be estimated.

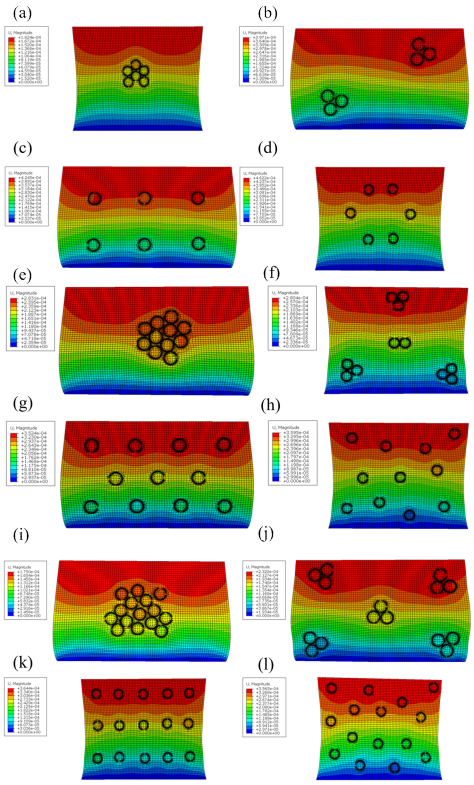

Fig. 6 Idealized finite element models for 100 nm silica particles at different loadings: (a)–(d) 3 wt%, (e)–(h) 5 wt%, and (i)–(l) 7 wt%, representing dispersion states from agglomerated to uniform.

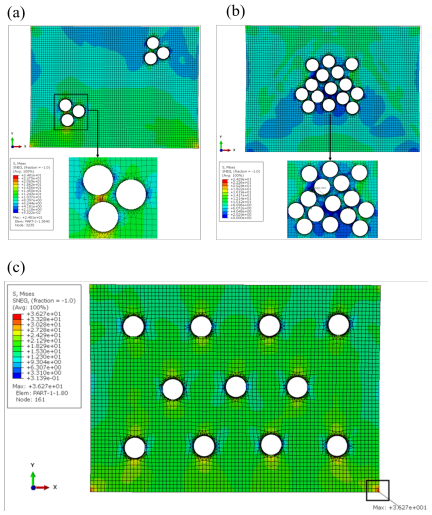

Fig. 7 Von Mises stress distributions of representative idealized models: (a) Intermediate phase (I), (b) Large Spherical cluster (LS), and (c) Uniform distribution (U).

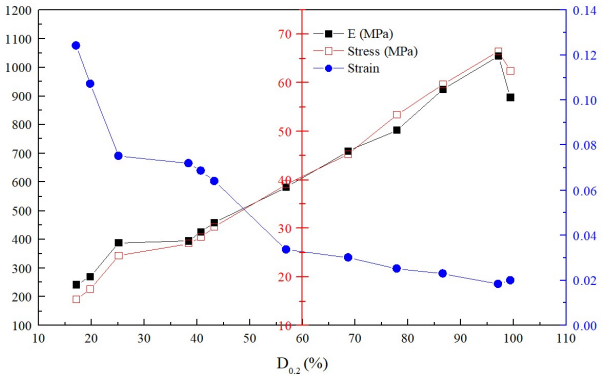

Fig. 8 Dependence of Young's modulus, tensile stress, and strain on $D_{0.2}$.

The finite element analysis employed in this study successfully predicted the mechanical strength of the PMMA/SiO_2 composites, demonstrating high consistency with experimental observations. These simulation results elucidate the critical role of particle dispersion in the reinforcement mechanism; specifically, well-dispersed silica nanoparticles function as effective physical barriers that impede crack propagation. By forcing cracks to deflect and traverse a more tortuous path around the particles, the onset of catastrophic failure is delayed, and the energy required for fracture is significantly increased. This confirmation of the crack path extension mechanism underscores that optimizing particle dispersion is not merely a strategy for defect avoidance but a fundamental requirement for maximizing stress-transfer efficiency and achieving the composite material's ultimate mechanical potential.

Although these findings are based on 2D microstructural models, which naturally simplify the complex 3D spatial connectivity and out-of-plane geometric features of nanoparticle clusters, the strong correlation observed between our FEA predictions and experimental data supports this approach as a statistically representative tool for understanding dispersion-performance relationships. Moreover, these results have important implications for the long-term performance of biomedical implants. In a physiological environment with cyclic loading, the stress-concentration points at local agglomerates are likely critical sites for fatigue crack initiation. By showing that a uniform dispersion (high $D_{0.2}$) reduces these local stress concentrations and encourages a tortuous crack path, this study offers a theoretical basis for improving the fatigue resistance and durability of PMMA-based bone cements, thereby decreasing the risk of early clinical failure such as aseptic loosening.

CONCLUSIONS

This study successfully synthesized PMMA/SiO_2 nanocomposites via the in situ sol-gel method, establishing robust organic-inorganic interfacial bonding, as confirmed by EDS and Raman spectroscopy. By integrating experimental tensile testing with microstructural analysis, a quantitative dispersion index ($D_{0.2}$) based on Voronoi tessellation was defined to rigorously evaluate particle distribution. The experimental results demonstrated a pronounced positive correlation between this dispersion index and the composite's mechanical properties, including Young's modulus, tensile strength, and fracture strain. This correlation substantiates that the enhancement of macroscopic mechanical performance is intrinsically linked to the uniformity of the inorganic filler distribution within the polymer matrix.

FEA based on real microstructures provided critical insights into the underlying failure mechanisms governing these improvements. The simulations revealed that mechanical failure is driven by a competition between defect-induced stress concentrations and reinforcement toughening. In systems characterized by poor dispersion, local agglomerates and the narrow ligaments between closely spaced particles acted as critical stress concentration sites, leading to premature brittle failure. Conversely, uniform dispersion facilitated effective stress transfer across the matrix, mitigating extreme local stress peaks and allowing the material to sustain higher loads. Furthermore, the development of idealized finite element models enabled the isolation of dispersion effects, predicting that achieving a theoretically perfect dispersion ($D_{0.2} \approx 100$ %) would elevate the mechanical potential of the composites significantly beyond the current experimental values.

Ultimately, while acknowledging that 2D SEM-based models inherently simplify the 3D spatial

connectivity of fillers, the high consistency between the FEA predictions and experimental observations validates the reinforcement mechanism where well-dispersed silica nanoparticles function as physical barriers to crack propagation. The simulations clarified that by forcing cracks to deflect and traverse a more tortuous path, the onset of catastrophic failure is delayed, and the energy required for fracture is increased. This confirms that optimizing particle dispersion is not merely a strategy for defect avoidance but a fundamental requirement for maximizing stress transfer efficiency. These findings provide a robust predictive framework for designing high-performance nanocomposites, highlighting the pivotal role of microstructural control in achieving the ultimate mechanical limits of organic-inorganic hybrid materials.

ACKNOWLEDGMENT

This work was supported by the National Science and Technology Council (NSTC), Taiwan, under Grant Nos. 112-2221-E-006-173, 113-2221-E-006-087-MY2,113-2221-E-006-112-MY 2, and 113-2221-E-006-116. The authors gratefully acknowledge the Core Facility Center at National Cheng Kung University, Taiwan, for providing access to the EM000800 and SQUID000200 instruments, which were funded by the NSTC project 114-2740-M-006-001. Additional support from the Higher Education Sprout Project of the Ministry of Education, Taiwan, through the Headquarters of University Advancement at National Cheng Kung University (NCKU), is also gratefully acknowledged.

REFERENCES

Abhiram, B., & Ghosh, D. (2023). Influence of nanofiller agglomeration on fracture properties of polymer nanocomposite: Insights from atomistic simulation. *Engineering Fracture Mechanics*, *290*, 109503.

Bistolfi, A., Ferracini, R., Albanese, C., Vernè, E., & Miola, M. (2019). PMMA-based bone cements and the problem of joint arthroplasty infections: status and new perspectives. *Materials*, *12*(23), 4002.

Bokobza, L. (2023). Elastomer nanocomposites: Effect of filler–matrix and filler–filler interactions. *Polymers*, *15*(13), 2900.

Chrispin Laila, A., Narayanan, M., Bhadrakumar Sindhu, D., & AlbyRoy, A. (2022). Mechanical properties of polymer matrix/glass fiber composites containing metal/hybrid nanoparticles-an overview. *High Performance Polymers*, *34*(8), 859-870.

Grove, B., Patton, D., & Ma, B. (2025). Microscopic-to-macroscopic finite element analysis for predicting polymer-graphene nanocomposite laminate mechanical strength. *Polymer Composites*, *46*, S40-S53.

Jaeblon, T. (2010). Polymethylmethacrylate: properties and contemporary uses in orthopaedics. *JAAOS-Journal of the American Academy of Orthopaedic Surgeons*, *18*(5), 297-305.

Jiang, C.-E., Chen, G.-Y., & Shi, S.-C. (2025). Sol-Gel Derived SiO_2/PMMA Composite Coatings with Tunable Dispersion for Corrosion Protection of Ti-6Al-4V. *Journal of the Chinese Society of Mechanical Engineers*, 467-474.

Karbowniczek, J. E., Ura, D. P., & Stachewicz, U. (2022). Nanoparticles distribution and agglomeration analysis in electrospun fiber based composites for desired mechanical performance of poly (3-hydroxybuty-rate-co-3-hydroxyvalerate (PHBV) scaffolds with hydroxyapatite (HA) and titanium dioxide (TiO2) towards medical applications. *Composites Part B: Engineering*, *241*, 110011.

Karpiński, R., & Szabelski, J. (2025). Mechanical properties and functional assessment of PMMA bone cements modified with glassy carbon. *Journal of Functional Biomaterials*, *16*(7), 254.

Kontou, E., Christopoulos, A., Koralli, P., & Mouzakis, D. E. (2023). The effect of silica particle size on the mechanical enhancement of polymer nanocomposites. *Nanomaterials*, *13*(6), 1095.

Li, H., Cheng, B., Gao, W., Feng, C., Huang, C., Liu, Y., Lu, P., & Zhao, H. (2022). Recent research progress and advanced applications of silica/polymer nanocomposites. *Nanotechnology Reviews*, *11*(1), 2928-2964.

Nguyen, N., Maloney, W., & Dauskardt, R. (1997). Reliability of PMMA bone cement fixation: fracture and fatigue crack-growth behaviour. *Journal of Materials Science: Materials in Medicine*, *8*(8), 473-483.

Race, A., & Mann, K. A. (2008). Fatigue crack propagation rates in PMMA bone cement cannot be reduced to a single power law. *Journal of Biomedical Materials Research Part B: Applied Biomaterials: An Official Journal of The Society for Biomaterials, The Japanese Society for Biomaterials, and The Australian Society for Biomaterials and the Korean Society for Biomaterials*, *86*(1), 278-282.

Ramanathan, S., Lin, Y.-C., Thirumurugan, S., Hu, C.-C., Duann, Y.-F., & Chung, R.-J. (2024). Poly (methyl methacrylate) in orthopedics: strategies, challenges, and prospects in bone tissue engineering. *Polymers*, *16*(3), 367.

Shi, S.-C., Chen, T.-H., & Mandal, P. K. (2020). Enhancing the mechanical and tribological properties of cellulose nanocomposites with aluminum nanoadditives. *Polymers*, *12*(6), 1246.

Shi, S.-C., & Zeng, X.-X. (2022). Effect of the strengthening mechanism of SiO2 reinforced poly (methyl methacrylate) on ductility performance. *Journal of Polymer Research*, *29*(10), 408.

Sui, Y., Cui, Y., Meng, X., & Zhou, Q. (2022). Research progress on the correlation between properties of nanoparticles and their dispersion states in polymer matrix. *Journal of applied polymer science*, *139*(19), 52096.

Szczęsny, G., Kopec, M., Politis, D. J., Kowalewski, Z. L., Łazarski, A., & Szolc, T. (2022). A review on biomaterials for orthopaedic surgery and traumatology: from past to present. *Materials*, *15*(10), 3622.

Szoradi, G. T., Feier, A. M., Zuh, S. G., Russu, O. M., & Pop, T. S. (2024). Polymethyl Methacrylate Bone Cement Polymerization Induced Thermal Necrosis at the Cement–Bone Interface: A Narrative Review. *Applied Sciences*, *14*(24), 11651.

Van Vugt, T. A., Arts, J. J., & Geurts, J. A. (2019). Antibiotic-loaded polymethylmethacrylate beads and spacers in treatment of orthopedic infections and the role of biofilm formation. *Frontiers in microbiology*, *10*, 1626.

Zhong, Y., Chen, Y., Zhang, M., Zhang, H., Liao, X., Jin, H., Feng, J., & Qin, X. (2025). Amplifying Effect in the Size Statistics of the Residual Particles and Its Applications in Analyzing Nanoparticle Dispersion in Polymer Nanocomposites. *Analytical Chemistry*, *97*(14), 7808-7813.

Zhu, F., Zhao, J., Duan, L., & Zhuang, B. (2025). Microscopic finite element modeling and fracture properties of particulate filled polymer composites. *Polymer Composites*, *46*(8), 7012-7026.